Loss of *Goosecoid-like* and *DiGeorge syndrome critical region 14* in interpeduncular nucleus results in altered regulation of rapid eye movement sleep

Hiromasa Funato[a,b,1], Makito Sato[a,1], Christopher M. Sinton[c], Laurent Gautron[c], S. Clay Williams[a], Amber Skach[a], Joel K. Elmquist[c], Arthur I. Skoultchi[d], and Masashi Yanagisawa[a,b,e,2]

Departments of [a]Molecular Genetics and [c]Internal Medicine and [e]Howard Hughes Medical Institute, University of Texas Southwestern Medical Center, Dallas, TX 75390; [b]Center for Behavioral Molecular Genetics, University of Tsukuba, Tsukuba 305-8575, Japan; and [d]Department of Cell Biology, Albert Einstein College of Medicine, Bronx, NY 10461

Contributed by Masashi Yanagisawa, August 27, 2010 (sent for review May 12, 2010)

Sleep and wakefulness are regulated primarily by inhibitory interactions between the hypothalamus and brainstem. The expression of the states of rapid eye movement (REM) sleep and non-REM (NREM) sleep also are correlated with the activity of groups of REM-off and REM-on neurons in the dorsal brainstem. However, the contribution of ventral brainstem nuclei to sleep regulation has been little characterized to date. Here we examined sleep and wakefulness in mice deficient in a homeobox transcription factor, *Goosecoid-like* (*Gscl*), which is one of the genes deleted in DiGeorge syndrome or 22q11 deletion syndrome. The expression of *Gscl* is restricted to the interpeduncular nucleus (IP) in the ventral region of the midbrain–hindbrain transition. The IP has reciprocal connections with several cell groups implicated in sleep/wakefulness regulation. Although $Gscl^{-/-}$ mice have apparently normal anatomy and connections of the IP, they exhibited a reduced total time spent in REM sleep and fewer REM sleep episodes. In addition, $Gscl^{-/-}$ mice showed reduced theta power during REM sleep and increased arousability during REM sleep. $Gscl^{-/-}$ mice also lacked the expression of *DiGeorge syndrome critical region 14* (*Dgcr14*) in the IP. These results indicate that the absence of *Gscl* and *Dgcr14* in the IP results in altered regulation of REM sleep.

homeobox transcription factor | mouse behavior | ventral brainstem

In vertebrates and invertebrates, sleep is defined behaviorally as a reversible quiescence which is regulated in a circadian and homeostatic manner, accompanied by an increased threshold to respond to external stimuli (1). In mammals and birds, sleep is classified further into rapid eye movement (REM) sleep and non-REM (NREM) sleep based on specific brain-activity patterns and muscle tonus detected by electroencephalography/electromyography (EEG/EMG). In rodents, NREM sleep is defined by high-amplitude, low-frequency waves on the EEG, typified by the presence of the 1- to 4-Hz (i.e., delta) frequencies. In contrast, REM sleep is characterized by power in the 6- to 12-Hz (i.e., theta) frequency band, which is derived primarily from hippocampal activity, combined with a loss of skeletal muscle tone. Switching between the sleeping and wakeful states is regulated primarily by inhibitory interactions between the hypothalamus and brainstem (2, 3). Switching between NREM and REM states is regulated further by inhibitory interactions between populations of neurons in the brainstem (3, 4). Although dopaminergic neurons in the ventral midbrainstem have been implicated in regulating sleep and wakefulness (5), the role of the ventral brainstem in sleep regulation has not been as well studied as the role of the dorsal brainstem.

It has been reported that lesions of the bilateral fasciculus retroflexus, a major input to the interpeduncular nucleus (IP), result in reduced REM sleep time (6, 7). The IP is located on the midline in the ventral region of the midbrain–hindbrain transition and is evolutionarily conserved from fish to mammals. It has reciprocal connections with the median raphe nucleus (MnR), dorsal raphe nucleus (DRN), laterodorsal tegmental nucleus (LDTg), and nucleus incertus (NI) (8–13), which are implicated in the regulation of sleep and wakefulness and the generation of hippocampal theta waves (2, 3, 14, 15). In addition, the IP receives input from the basal forebrain via the fasciculus retroflexus directly or relayed at the medial habenular nucleus. In turn, the IP innervates the basal forebrain (16). Because the basal forebrain is known to regulate the vigilance state, this reciprocal pattern of innervation also supports a potential role of the IP in sleep mechanisms.

However, no studies to date have examined whether the IP is involved in sleep, in part because the size and position of the IP make it difficult to lesion the IP or inject it locally without damaging bilateral dorsal brainstem nuclei and fibers of passage. A recent comprehensive approach to gene expression in the mouse brain revealed that a homeobox transcription factor *Goosecoid-like* (*Gscl*), also known as "*Gsc2*," has an expression pattern restricted to the IP (17). *Gscl* is one of the genes deleted in patients who have DiGeorge syndrome or 22q11 deletion syndrome, who have a variety of psychiatric symptoms (18). We thus examined sleep/wakefulness parameters in $Gscl^{-/-}$ mice (19) under baseline conditions and also studied REM sleep rebound after REM sleep deprivation and the sensory threshold to arousal during sleep in these mice.

Results

***Gscl* Expression Is Restricted to the IP.** We examined the expression pattern of *Gscl* mRNA at different developmental stages. In the adult brain, *Gscl* mRNA is expressed exclusively in the caudal (IPc) and lateral (IPl) subnuclei of IP (Fig. 1 *A* and *B*). During embryonic development, the expression of *Gscl* mRNA is restricted to the developing ventral midbrain/pons transitional region, a future IP region (Fig. 1 *C* and *D*), as reported previously (17, 20). Loss of *Gscl* does not alter subnuclear structures in the Nissl-stained IP, and there is no difference in position and proportion between *Gscl*-positive and *Gscl*-negative subnuclei.

IP neurons contain several inhibitory neurotransmitters, including GABA, somatostatin, and substance P, and the IP receives projections of cholinergic, serotonergic, and substance P-containing fibers (9, 16, 21). We examined whether the loss of *Gscl* alters the neurochemical characteristics of the IP neurons and the input fibers. When $Gscl^{+/-}$ mice were crossed with the *Gad67-Gfp* knock-in line (22), $Gscl^{-/-}$; $Gad67^{Gfp/+}$ mice showed diffuse and moderate GFP expression in the entire IP with strong expression in the rostral subnucleus, similar to $Gscl^{+/+}$; $Gad67^{Gfp/+}$ mice (Fig. 1 *E* and *F*).

Author contributions: H.F., M.S., and M.Y. designed research; H.F., M.S., L.G., S.C.W., and A.S. performed research; A.I.S. contributed new reagents/analytic tools; H.F., M.S., C.M.S., and J.K.E. analyzed data; and H.F. and M.Y. wrote the paper.

The authors declare no conflict of interest.

[1]H.F. and M.S. contributed equally to this work.

[2]To whom correspondence should be addressed. E-mail: masashi.yanagisawa@utsouthwestern.edu.

NEUROSCIENCE

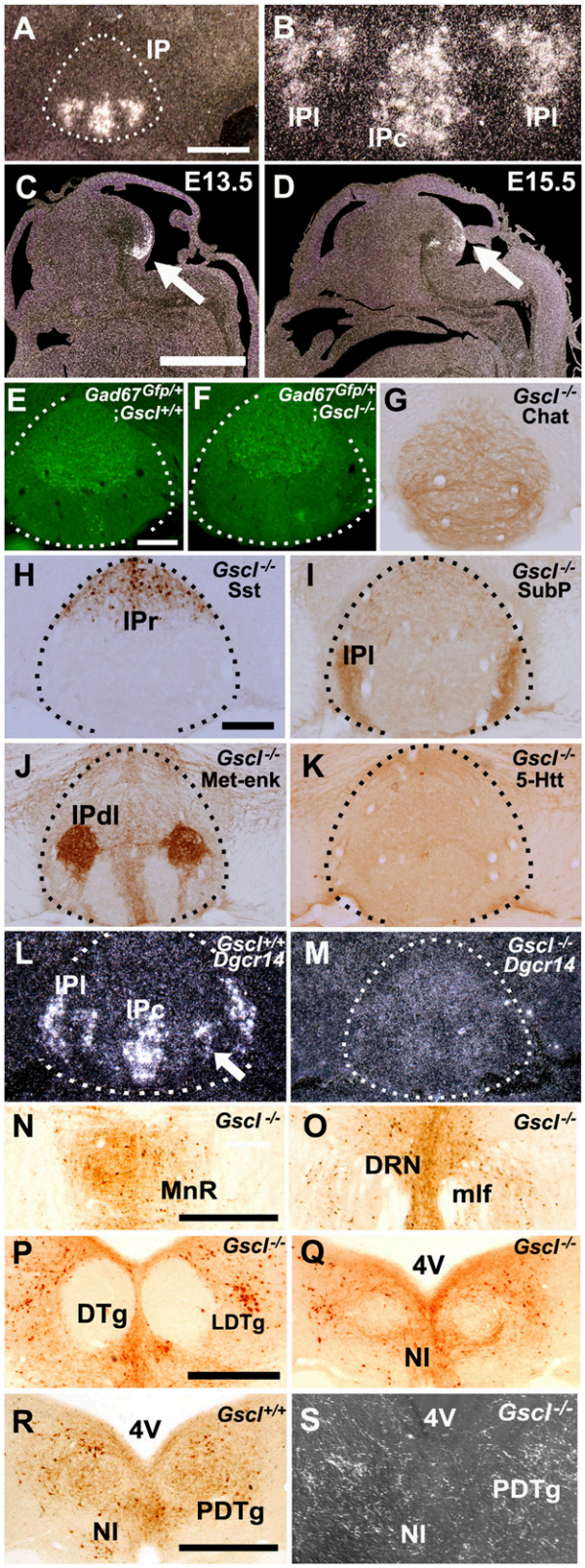

Fig. 1. Normal anatomical structure of the IP of a *Gscl*-deficient mouse. (*A*) *Gscl* mRNA expression is restricted to the IP (delineated by broken lines). (*B*) High-magnification view of *A* shows that *Gscl* mRNA is expressed in the IPc and IPl. (*C* and *D*) During the embryonic stage, *Gscl* mRNA expression is restricted to the developing ventral midbrain/pons transition (arrow). (*E* and *F*) Both $Gscl^{+/+}$; $Gad67^{Gfp/+}$ and $Gscl^{-/-}$; $Gad67^{Gfp/+}$ mice have diffuse and moderate GFP expression in the entire IP (delineated by broken lines) with strong expression in the rostral subnucleus. (*G*–*K*) The IP of $Gscl^{-/-}$ mice exhibits immunoreactivities for ChAT (*G*), somatostatin (Sst) (*H*), substance P (SubP) (*I*), Met-enkephalin (Met-enk) (*J*), and 5-HT transporter (5-HTT) (*K*). (*L*) $Gscl^{+/+}$ mice have marked expression of *Dgcr14* in the IPc, IPl, and part of the intermediate subnucleus (arrow). (*M*) $Gscl^{-/-}$ mice did not show increased expression of *Dgcr14* mRNA in the IP subnucleus. (*N*–*R*) Retrograde tracing from the IP after injection of a retrograde tracer, cholera toxin B, in the IPl. Labeled fibers and cells were recognized in the MnR (*N*), DRN (*O*), LDTg (*P*), and NI (*Q*) of $Gscl^{-/-}$ mice and in the NI of $Gscl^{+/+}$ mice (*R*). (*S*) Injection of an anterograde tracer, AAV-GFP, in the IPl revealed GFP-positive fibers in the PDTg and NI of $Gscl^{-/-}$ mice. mlf, medial longitudinal fasciculus. (Scale bars: 300 μm in *A*, *C*, *N*, P, and *R*; 150 μm in *E* and *H*.)

Consistent with the previous reports on wild-type mice (9, 16, 21), both $Gscl^{-/-}$ and $Gscl^{+/+}$ mice showed (*i*) diffuse choline acetyltransferase (ChAT) immunoreactivity in the IP (Fig. 1*G*); (*ii*) strong somatostatin immunoreactivity in the rostral and apical subnuclei (Fig. 1*H*); (*iii*) moderate substance P immunoreactivity in the IP with prominent immunoreactivity in the lateral subnucleus (Fig. 1*I*); (*iv*) Met-enkephalin immunoreactivity strongly in the dorsolateral subnucleus and moderately in the rostral and caudal subnuclei (Fig. 1*J*); and (*v*) diffuse serotonin (5-HT) transporter immunoreactivity in the entire IP with scattered strong immunoreactive cells (Fig. 1*K*). Loss of *Gscl* had no appreciable effects on *Gad67-Gfp* expression, or immunoreactivity for ChAT, somatostatin, substance P, and 5-HT transporter outside the IP. We also examined the expression of *DiGeorge syndrome critical region 14 (Dgcr14*, also known as "*Es2*") mRNA, a gene adjacent to *Gscl* on both the human and mouse chromosomes. In the $Gscl^{+/+}$ mouse brain, *Dgcr14* mRNA was strongly expressed in the IPc, IPl, and a part of the intermediate subnuclei (Fig. 1*I*), similar to the expression pattern of *Gscl* mRNA in the IP (Fig. 1*B*). $Gscl^{-/-}$ mice, however, lacked the expression of *Dgcr14* mRNA in the IP (Fig. 1*J*). In contrast to *Gscl* mRNA, *Dgcr14* mRNA showed a diffuse and weak expression pattern in the entire brain of wild-type mice; this diffuse expression was conserved in $Gscl^{-/-}$ mice.

To examine whether loss of *Gscl* affected fiber connections to the IP, we injected a retrograde tracer, cholera toxin B, into the lateral subnucleus of the IP. Labeled cells were recognized in the MnR (Fig. 1*K*), DRN (Fig. 1*L*), LDTg (Fig. 1*M*), NI (Fig. 1*N*), median septal nucleus, nucleus of the diagonal band, lateral hypothalamus, supramammillary nucleus, and medial habenular nucleus of $Gscl^{-/-}$ mice. These nuclei were the same as those previously described in wild-type mice (Fig. 1*O*) (8–10, 12, 13, 23). Injection of an anterograde tracer, an adeno-associated viral vector containing the gene for GFP (AAV-GFP), in the IPl of $Gscl^{-/-}$ and $Gscl^{+/+}$ mice showed dense efferent fibers throughout pontine midline structures, including the MnR, DRN, LDTg, NI, and posterodorsal tegmental nucleus (PDTg) (Fig. 1*P*), as previously described (8, 9, 11). Thus, we found no apparent differences between the two genotypes in the afferent and efferent fiber connections to and from the IP, although there were small differences in the number of labeled cells and fibers among all tracer-injected brains because of inevitable differences in the exact locations and amounts of tracer injected.

***Gscl*-Deficient Mice Show Reduced REM Sleep Time.** $Gscl^{-/-}$ mice exhibited a decrease in both total time and episode frequency of REM sleep during the light period and over 24 h when compared with $Gscl^{+/+}$ mice (Fig. 2 and Table 1). However, no significant difference was noted in the duration of REM sleep episodes in $Gscl^{-/-}$ and $Gscl^{+/+}$ mice (Table 1). REM sleep latency was increased during the light period and over 24 h in $Gscl^{-/-}$ mice. In addition to a slight but significant increase in total NREM sleep time, $Gscl^{-/-}$ mice exhibited a longer mean duration and reduced frequency of NREM sleep episodes when compared with wild-type mice during the light period and over 24 h (Table 1). This obser-

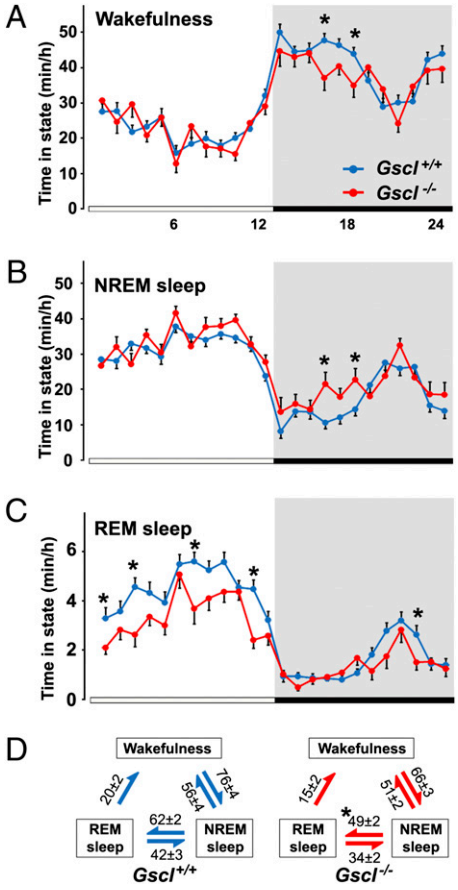

Fig. 2. Sleep and wakefulness in *Gscl*-deficient mice. (*A*–*C*) Circadian variation in wakefulness, NREM sleep, and REM sleep in $Gscl^{+/+}$ (n = 12) and $Gscl^{-/-}$ mice (n = 6). Data (mean ± SEM) are expressed as minutes per hour spent in each stage, averaged from EEG/EMG recordings during three consecutive 24-h periods. (*D*) Values indicate the number (mean ± SEM) of transitions between wakefulness, NREM sleep, and REM sleep per 24 h. $Gscl^{-/-}$ mice (*Right*) showed reduced transitions from NREM sleep to REM sleep compared with $Gscl^{+/+}$ mice (*Left*). Data (mean + SEM) were subjected to ANOVA with repeated measurements followed by the Tukey post hoc test. *$P < 0.05$.

vation indicates that the NREM sleep phase is more consolidated in the light period in $Gscl^{-/-}$ mice than in $Gscl^{+/+}$ mice. Wakefulness time and mean episode duration were similar in $Gscl^{-/-}$ and wild-type mice, although we noted a tendency toward shorter total wakefulness time during the dark period in $Gscl^{-/-}$ mice (Fig. 2 and Table 1). Importantly, the number of transitions from NREM sleep to REM sleep was reduced selectively in $Gscl^{-/-}$ mice (Fig. 2*D*). This finding is consistent with a reduced number of REM sleep episodes, a shorter total REM sleep time, and longer duration of NREM sleep episodes. In other words, $Gscl^{-/-}$ mice tend to "skip" REM sleep episodes during NREM sleep.

Reduced Theta Power in *Gscl*-Deficient Mice. EEG spectral analysis of $Gscl^{+/+}$ and $Gscl^{-/-}$ mice during wakefulness, NREM sleep, and REM sleep revealed that EEG power density in the theta frequency range (6–12 Hz) during REM sleep was reduced significantly in $Gscl^{-/-}$ mice compared with $Gscl^{+/+}$ mice (P = 0.002) (Fig. 3). In addition, we noted that EEG power density in the delta frequency range (1–4 Hz) during NREM sleep was greater in $Gscl^{-/-}$ mice than in $Gscl^{+/+}$ mice (P = 0.03) (Fig. 3).

Increased Arousability During REM Sleep in *Gscl*-Deficient Mice. While making vigilance-state recordings in $Gscl^{-/-}$ mice, we observed that $Gscl^{-/-}$ mice seemed excessively sensitive to external stimuli during sleep. To examine the arousability of $Gscl^{-/-}$ mice, we tested their arousal threshold during REM and NREM sleep using acoustic stimuli. In 14 of 17 trials during REM sleep, $Gscl^{-/-}$ mice (n = 4) were awakened in response to a standardized acoustic stimulus, but $Gscl^{+/+}$ mice (n = 5) remained asleep in 12 of 13 trials ($P < 0.001$; Fig. 4*A*). In contrast, there was no significant difference in the arousal response to acoustic stimuli during NREM sleep (P = 0.2). To confirm this finding with a different modality of stimuli, we measured the time to awaken in response to combined acoustic, olfactory, and visual stimuli caused by moving a Latex glove close to a mouse. $Gscl^{-/-}$ mice had significantly shorter latencies to awake than $Gscl^{+/+}$ mice during REM sleep (Fig. 4*B*).

Reduced REM Sleep Rebound in *Gscl*-Deficient Mice. To examine the homeostatic regulation of REM sleep, $Gscl^{-/-}$ mice were deprived of REM sleep from Zeitgeber time (ZT)6 to ZT12, and their REM sleep time then was examined from ZT12 to ZT24, when there was no significant difference between $Gscl^{+/+}$ and $Gscl^{-/-}$ mice in baseline REM sleep time (Fig. 2*C*). After REM sleep deprivation, both $Gscl^{+/+}$ and $Gscl^{-/-}$ mice spent longer in REM sleep than under baseline conditions (Fig. 5*A*), but both the extent and duration of the REM sleep rebound were less in $Gscl^{-/-}$ mice than $Gscl^{+/+}$ mice. REM sleep deprivation did not affect NREM sleep time in either genotype (Fig. 5*B*).

Discussion

The present study has shown that $Gscl^{-/-}$ mice spend less time in REM sleep, express fewer REM sleep episodes, and have fewer transitions from NREM sleep to REM sleep. Furthermore, these mice have reduced theta power and increased arousability during REM sleep. In view of the restricted expression of *Gscl* to the IP combined with a specific loss of expression of *Dgcr14* in the IP of $Gscl^{-/-}$ mice, these results indicate that the normal function of the IP is required for REM sleep regulation.

Although $Gscl^{-/-}$ mice showed reduced theta power, the EEG pattern of REM sleep still was clearly different from that of NREM sleep and of wakefulness. Moreover, we staged REM sleep based on both the appearance of theta wave and loss of muscle tone. Thus, it is unlikely that shorter total time of REM sleep or reduced REM sleep rebound of $Gscl^{-/-}$ mice resulted from a misscoring of REM sleep.

The IP is located at the ventral region of the midbrain–hindbrain transition and has afferent and efferent connections with the basal forebrain and brainstem. These connections suggest that the IP may function as an interface between the basal forebrain and brainstem in the modulation of brain function and behavior. Although the functional role of the IP remains unknown (16), several findings have suggested that the IP may be associated with sleep and wakefulness. Unlike most brain regions, glucose utilization in the IP is increased during REM sleep as well as under anesthesia (24–26). Moreover, bilateral lesions of the fasciculus retroflexus, the major afferent path from the IP, decrease the time spent in REM sleep (6, 7). To date, however, no report has directly examined the role of the IP in sleep mechanisms, primarily because research has tended to focus on the dorsal region of the brainstem (2–4) and because surgical procedures targeting the IP inevitably damage bilateral dorsal brainstem nuclei as well as fibers connecting the hypothalamus with the brainstem nuclei.

Among IP subnuclei, *Gscl* and *Dgcr14* are expressed mainly in the IPc and IPl structures. These subnuclei send efferent fibers containing serotonergic REM-off neurons to the MnR and DRN and efferent fibers containing cholinergic REM-on neurons to the LDTg (3, 9, 11, 27). In addition, the IPc and IPl subnuclei send efferent fibers to the NI (8, 9, 11), which relays ascending projections from the nucleus pontis oralis to the medial septal nucleus, a pathway implicated in hippocampal theta generation (14). Moreover, the IP sends a small number of efferent fibers to the

Table 1. Sleep/wakefulness parameters

Period	Wakefulness			NREM sleep			REM sleep		
	Gscl$^{+/+}$	*Gscl*$^{-/-}$	*P*	*Gscl*$^{+/+}$	*Gscl*$^{-/-}$	*P*	*Gscl*$^{+/+}$	*Gscl*$^{-/-}$	*P*
24 h									
Time (min)	764 ± 11	730 ± 20	0.071	596 ± 10	**649 ± 19**	0.011	79.6 ± 2.6	**61.0 ± 2.3**	<0.0001
Duration (s)	686 ± 46	689 ± 42	0.965	318 ± 11	**400 ± 17**	0.0002	77.6 ± 1.8	74.5 ± 2.1	0.303
Frequency (episode/h)	2.36 ± 0.14	**1.84 ± 0.08**	0.003	4.01 ± 0.15	**3.17 ± 0.07**	<0.0001	2.17 ± 0.08	**1.63 ± 0.06**	<0.0001
REM sleep latency (min)							8.13 ± 0.25	**10.8 ± 0.43**	<0.0001
12-h light period									
Time (min)	275 ± 8.0	273 ± 5.9	0.88	385 ± 6.4	**402 ± 6.0**	0.066	60.0 ± 2.6	**44.7 ± 2.0**	<0.0001
Duration (s)	519 ± 39	579 ± 41	0.35	325 ± 12	**430 ± 22**	0.0001	81.6 ± 2.3	79.6 ± 2.6	0.602
Frequency (episode/h)	2.36 ± 0.13	**1.79 ± 0.10**	0.001	4.99 ± 0.16	**3.74 ± 0.12**	<0.0001	3.16 ± 0.15	**2.26 ± 0.09**	<0.0001
REM sleep latency (min)							8.17 ± 0.28	**10.8 ± 0.46**	<0.0001
12-h dark period									
Time (min)	490 ± 9.0	457 ± 16	0.054	210 ± 8.8	**247 ± 15**	0.032	19.5 ± 0.99	16.4 ± 1.1	0.059
Duration (s)	981 ± 91	850 ± 67	0.26	311 ± 14	**366 ± 13**	0.009	70.8 ± 2.1	65.5 ± 2.0	0.085
Frequency (episode/h)	2.34 ± 0.18	1.93 ± 0.12	0.075	3.02 ± 0.19	2.59 ± 0.15	0.087	1.17 ± 0.06	0.98 ± 0.07	0.065
REM sleep latency (min)							8.11 ± 0.29	**11.0 ± 0.61**	0.0003

Data are expressed as mean ± SEM for *Gscl*$^{+/+}$ mice (n = 12) and *Gscl*$^{-/-}$ mice (n = 6). All parameters were derived from EEG/EMG recordings for three consecutive 24- h periods. Statistical comparisons are by Student's t test. Significant changes ($P < 0.05$) are shown in bold type.

hippocampus and medial septal nucleus (9, 11). These connections provide an anatomical basis for the IP as a regulator of hippocampal theta and REM sleep.

Another interesting phenotype of *Gscl*$^{-/-}$ mice is increased arousability, specifically during REM sleep, in response to external stimuli. The elevated arousability is unlikely to be caused by disturbed peripheral sensory processing or increased anxiety, because *Gscl*$^{-/-}$ mice respond normally to acoustic or visual stimuli during NREM sleep and wakefulness and show normal anxiety behavior (28). External stimuli may activate wake-promoting neurons in the brainstem to switch from sleep to wakefulness (2, 29). Although the increased arousability of *Gscl*$^{-/-}$ mice suggests an altered regulation of wake-promoting neurons in response to sensory stimuli, further studies are needed to elucidate the detailed mechanisms.

Gscl$^{-/-}$ mice exhibited an REM sleep rebound after deprivation, but the magnitude and duration of the rebound was smaller than in wild-type mice. Because *Gscl*$^{-/-}$ mice spend less time in REM sleep than wild-type mice under baseline conditions, the reduced REM sleep rebound may result from a smaller need for REM sleep in *Gscl*$^{-/-}$ mice after 6 h of REM sleep deprivation. However, it also is possible that the mechanisms of REM sleep rebound per se are affected in the knock-out mice.

The accentuated expression in the IP of *Dgcr14* was absent in *Gscl*$^{-/-}$ mice, in which the entire *Gscl* gene was replaced with the puromycin resistance and hygromycin resistance genes (19). Another strain of *Gscl*$^{-/-}$ mice, in which the entire *Gscl* gene was replaced with the neomycin resistance gene, also showed a loss of *Dgcr14* expression in the IP (30). *Dgcr14* is located only 2 kb downstream of *Gscl*, with the same transcription direction, suggesting that *Gscl* contains a *cis* regulatory element required for the high expression of *Dgcr14* in IP subnuclei. Downstream of *Dgcr14* but in the opposite transcription direction are two genes, *Testis-specific serine kinase 1* (*Tssk1*) and *Tssk2*, that are expressed in the brain only in the piriform cortex [ref. 18 and Allen Brain Atlas (http://mouse.brain-map.org/)]. Hence, loss of *Gscl* and *Dgcr14* expression in the IP may be sufficient to cause the altered regulation of sleep/wakefulness behavior in *Gscl*$^{-/-}$ mice. Gscl is a paralogue of goosecoid and a homeobox transcription factor that recognizes a specific DNA sequence (31) and interacts with ring finger protein 4 (32). In addition, Dgcr14 is a nuclear protein with a coiled-coil domain (33). These findings suggest that loss of *Gscl* and *Dgcr14* may alter gene- or protein-expression profiles in the IPc and IPl subnuclei, resulting in a functional abnormality.

Gscl and *Dgcr14* are among the genes deleted in most individuals with DiGeorge syndrome or 22q11 deletion syndrome (20, 33). These patients have multiple neuropsychiatric symptoms and are susceptible to schizophrenia (18, 34, 35). Moreover, it has been reported that polymorphisms of *DGCR14* are significantly associated with schizophrenia (36). Interestingly, *Df(16)A*$^{+/-}$ mice with a microdeletion including the *Gscl* and *Dgcr14* genes showed reduced synchrony of hippocampal theta with the neuronal activity of the prefrontal cortex (37). Together with these findings, the present results suggest that loss of *Gscl* and *Dgcr14* affects the regulation of hippocampal theta and REM sleep, possibly contributing to the psychiatric symptoms frequently seen in patients who have 22q11 syndrome.

Materials and Methods

Animals. *Gscl*$^{-/-}$ mice and littermate *Gscl*$^{+/+}$ mice were derived from *Gscl*$^{+/-}$ parents that were backcrossed for more than six generations to the C57BL/6J strain (19). *Gad67*$^{Gfp/+}$ mice were previously described (22) and crossed to the

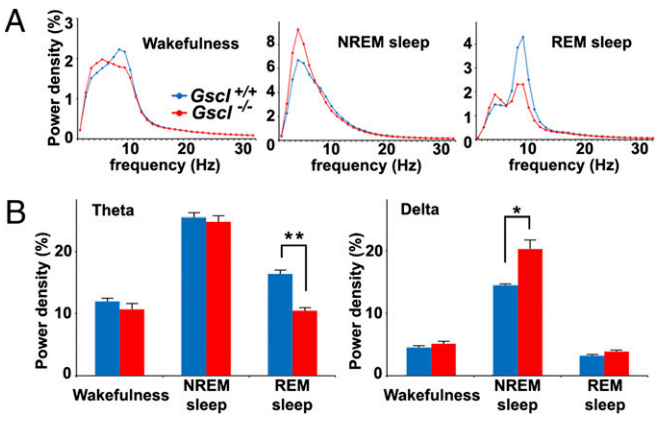

Fig. 3. EEG spectral analysis of *Gscl*$^{-/-}$ mice. (*A*) EEG spectral profiles of *Gscl*$^{+/+}$ mice (blue line, n = 12) and *Gscl*$^{-/-}$ mice (red line, n = 6) during wakefulness (*Left*), NREM sleep (*Center*), and REM sleep (*Right*). The average EEG spectra were normalized to total EEG power from 1–32 Hz in 1-Hz bins. (*B*) *Gscl*$^{-/-}$ mice (red bar) exhibited a reduced power density in the theta frequency band (*Left*) during REM sleep and a greater power density in the delta frequency band (*Right*) during NREM sleep, when compared with *Gscl*$^{+/+}$ mice (blue bar). Data (mean + SEM) were analyzed with ANOVA followed by the Tukey post hoc test. *$P < 0.05$; **$P < 0.005$.

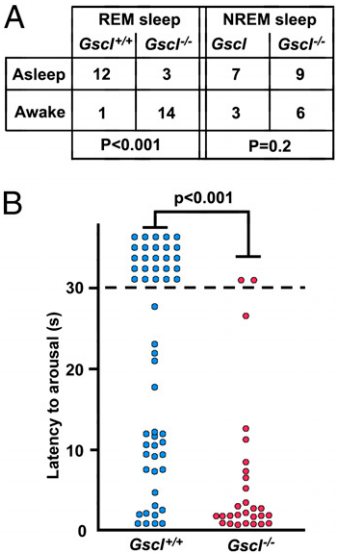

Fig. 4. Arousal response to stimuli during sleep. (*A*) (*Left*) During REM sleep, $Gscl^{-/-}$ mice (n = 4) tended to be awakened in response to acoustic stimuli, but $Gscl^{+/+}$ mice (n = 5) remained asleep (χ^2 test; $P < 0.001$). (*Right*) There was no significant difference between $Gscl^{-/-}$ mice and $Gscl^{+/+}$ mice in the arousal response to an approaching object during NREM sleep ($P = 0.2$). Numbers in the table denote the number of stimulus trials. (*B*) The latency of $Gscl^{-/-}$ mice (n = 4) in response to an approaching object during REM sleep was shorter than that of $Gscl^{+/+}$ mice (n = 5) (Mann–Whitney's u test, $P <$ 0.001). Circles represent individual trials.

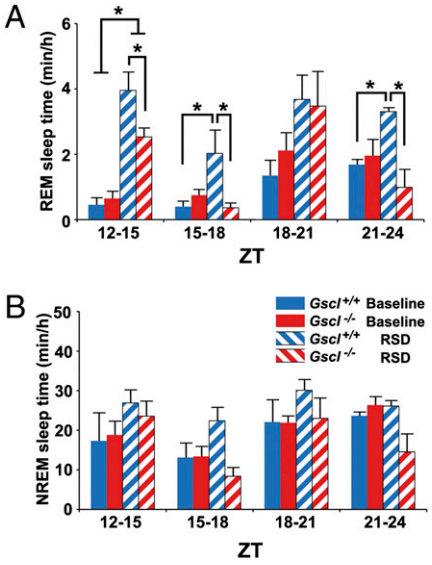

Fig. 5. REM sleep rebound after REM sleep deprivation. (*A*) After 6 h of REM sleep deprivation (RSD) from ZT6–12, the time spent in REM sleep is displayed for each 3-h period during the recovery phase from ZT12–24. Both $Gscl^{+/+}$ mice (n = 5) and $Gscl^{-/-}$ mice (n = 4) spent increased time in REM sleep from ZT12–15 compared with baseline. $Gscl^{-/-}$ mice exhibited a shorter REM sleep time than $Gscl^{+/+}$ mice during ZT12–15, ZT15–18, and ZT21–24. (*B*) The time spent in NREM sleep after 6 h of RSD for each 3-h period from ZT 12–24. RSD did not alter NREM time in either $Gscl^{+/+}$ or $Gscl^{-/-}$ mice. Data (mean ± SEM) were analyzed with ANOVA followed by the Tukey post hoc test. $^*P < 0.05$.

$Gscl^{+/-}$ line. Mice were provided food and water ad libitum, maintained on a 12-h light/dark cycle at all times, and were under controlled temperature and humidity conditions. All procedures were approved by the Institutional Animal Care and Use Committee of the University of Texas Southwestern Medical Center at Dallas and were carried out in strict accordance with the National Institute of Health Guide for the Care and Use of Laboratory Animals. Genotypes were determined by the amplification of genomic DNA by PCR.

EEG/EMG Electrode Implantation. For chronic EEG/EMG monitoring, 12- to 14-wk-old $Gscl^{-/-}$ and wild-type male mice were anesthetized with 40 mg/kg ketamine and 4 mg/kg xylazine, and the cranium was exposed. Four electrode pins were lowered to the dura under stereotaxic control, and two flexible wires for EMG recording were inserted in the neck muscle and then attached to the skull with dental cement. The electrodes for EEG signals were positioned over the frontal and occipital cortices [anteroposterior (AP): 0.5 mm, mediolateral (ML): 1.3 mm, dorsoventral (DV): −1.3 mm; and AP: −4.5 mm, ML: 1.3 mm, DV: −1.3 mm]. After recovery from anesthesia, the mice were housed individually and tethered to a counterbalanced arm (Instech Laboratories) that allowed the free movement and exerted minimal weight. All mice were allowed 14 d of recovery from surgery and habituation to the recording conditions.

EEG/EMG Analysis. EEG/EMG signal was recorded continuously for three consecutive 24-h periods. EEG/EMG signals were amplified using a Grass Model 78 (Grass Instruments), filtered (EEG: 0.3–300 Hz; EMG: 30–300 Hz), digitized at a sampling rate of 250 Hz, and displayed using custom polygraph software. The vigilance state in each 20-s epoch was classified as NREM sleep, REM sleep, or wakefulness by visual inspection of the EEG and EMG signals by two independent observers blinded as to genotype. Total time spent in wakefulness, NREM, and REM sleep was derived by summing the total number of 20-s epochs in each state. Mean episode durations were determined by dividing the total time spent in each state by the number of episodes of that state. Mean REM sleep latency was determined by averaging the time elapsed from the beginning of a continuous NREM sleep episode to the beginning of the subsequent REM sleep episode. Epochs containing movement artifacts were included in the state totals but excluded from subsequent spectral analysis. EEG signals were subjected to a fast Fourier transform analysis from 1 to 32 Hz with a 1-Hz bin using MatLab (MathWorks). EEG power density in each frequency bin was expressed as a percentage of the mean total EEG power over all frequency bins and vigilance states.

Arousability Test During REM and NREM Sleep. EEG/EMG-implanted 14- to 15-wk-old male mice were tested during the light period (ZT 6–10) in a cage equipped with a speaker. An experimenter monitored EEG/EMG signals in a room adjacent to the recording room. An 8-kHz, 70-dB, 500-ms pulse of a sinusoidal tone was delivered during NREM and REM sleep episodes. The number of trials in which mice reacted to the sound, as seen in robust EMG signals, were counted over the total number of trials. A similar study used a Latex glove attached to the end of a long metal rod as the external stimulus during videotape recording. Ten seconds after the onset of REM sleep under continuous EEG/EMG monitoring, an experimenter gently moved a glove from a distance of 3 m from the mouse to a distance of 5 cm. The latency to awaken was scored in real time from the onset of stimulus to apparent wakefulness as indicated by the EEG/EMG signals. All experiments were conducted by an experimenter who was blinded as to mouse genotype.

REM Sleep Deprivation. REM sleep deprivation was conducted for 6 h in the second half of the light period (ZT 6–12) by gentle handling under EEG/EMG monitoring. A REM transition was defined by the reduction of slow-wave amplitude and the appearance of theta wave intermixed with slow waves on the EEG, combined with diminishing EMG tonus. After REM sleep deprivation, the mice were kept in the same experimental cages with continuous recording of the EEG/EMG for a further 24 h. The vigilance state data during the recovery period were compared with baseline data recorded during the period before the deprivation procedure.

In Situ Hybridization and Histological Examinations. Animals were deeply anesthetized with ketamine and xylazine and then perfused with PBS, followed by 4% paraformaldehyde. Brains or embryos were removed, postfixed overnight in 4% paraformaldehyde, and then equilibrated in 20% sucrose for 2 d. The brains and embryos then were sectioned on a freezing microtome at 35 μm and mounted on Matsunami Adhesive Silane-coated slide glass (Matsunami Glass). The sections were hybridized in situ to ^{35}S-labeled *Gscl* or *Dgcr14* sense and antisense probes synthesized from pGEM-T Easy (Promega) containing the sequence of *Gscl* or *Dgcr14* mRNA, using a Maxiscript kit (Ambion) in the presence of ^{35}S-CTP (Amersham). The slides were developed in Kodak D-19 and counterstained using Nissl stain. After fixation and sectioning of $Gscl^{+/+}$; $Gad67^{Gfp/+}$ and $Gscl^{-/-}$; $Gad67^{Gfp/+}$ brains as above, GFP fluorescence was observed under the fluorescence microscope. Immunohistochemistry was performed using a free-floating method. The brain sections were incubated with antibodies for ChAT (goat polyclonal, AB144;

Millipore), somatostatin (rabbit polyclonal, AB5494; Millipore), substance P (rabbit polyclonal, AB1566; Millipore), Met-enkephalin (rabbit polyclonal, AB5026; Millipore), and 5-HT transporter (rabbit polyclonal, ab44520; Abcam) followed by incubation with biotinylated anti-rabbit or goat IgG, and then incubated in avidin–biotin–HRP conjugate (Vector). Positive immunoreactivity was visualized using 3,3′-diaminobenzidine (DAB).

Tracer Injection. Under anesthesia 12- to 14-wk-old *Gscl*$^{-/-}$ and wild-type male mice were placed in a stereotaxic apparatus, and a fine glass pipette was positioned in the lateral subnucleus at coordinates (AP: −3.5 mm, ML: 0.3 mm, DV: 4.8 mm) according to a mouse brain atlas (38). After the injection of tracer, the pipette was withdrawn slowly, and the incision was closed with sutures. The mouse survived for 7 d before being perfused with 4% paraformaldehyde. The brain then was processed for immunostaining.

As a retrograde tracer, 200 nL of 1% cholera toxin B (List Biotechnological Labs) was injected. Immunostaining was performed using anti-goat cholera toxin B antibody (List Biotechnological Labs) and DAB. As an anterograde tracer, 50–100 nL of AAV-GFP (Harvard Gene Therapy Initiative Research Vector Core Facility) was used. Brain sections were incubated with rabbit anti-GFP antibody (Molecular Probes). GFP-positive fibers were visualized with DAB and observed under dark-field microscopy.

ACKNOWLEDGMENTS. We thank Y. Yanagawa (Gunma University, Maebashi, Japan) for providing *Gad67* knock-in mice; C. Lee, S. Dixon, R. Floyd, and M. Thornton for technical support; T. Motoike, Y. Ikeda, H. Kumagai, I. Chang, A. Chang, S. Ogawa, J. Long, and A. Tsai for critical discussions and manuscript review. M.Y. is an Investigator of the Howard Hughes Medical Institute. This work was supported in part by the Perot Family Foundation.

1. Hendricks JC, Sehgal A, Pack AI (2000) The need for a simple animal model to understand sleep. *Prog Neurobiol* 61:339–351.
2. Saper CB, Chou TC, Scammell TE (2001) The sleep switch: Hypothalamic control of sleep and wakefulness. *Trends Neurosci* 24:726–731.
3. Pace-Schott EF, Hobson JA (2002) The neurobiology of sleep: Genetics, cellular physiology and subcortical networks. *Nat Rev Neurosci* 3:591–605.
4. Lu J, Sherman D, Devor M, Saper CB (2006) A putative flip-flop switch for control of REM sleep. *Nature* 441:589–594.
5. Monti JM, Monti D (2007) The involvement of dopamine in the modulation of sleep and waking. *Sleep Med Rev* 11:113–133.
6. Haun F, Eckenrode TC, Murray M (1992) Habenula and thalamus cell transplants restore normal sleep behaviors disrupted by denervation of the interpeduncular nucleus. *J Neurosci* 12:3282–3290.
7. Valjakka A, et al. (1998) The fasciculus retroflexus controls the integrity of REM sleep by supporting the generation of hippocampal theta rhythm and rapid eye movements in rats. *Brain Res Bull* 47:171–184.
8. Goto M, Swanson LW, Canteras NS (2001) Connections of the nucleus incertus. *J Comp Neurol* 438:86–122.
9. Groenewegen HJ, Ahlenius S, Haber SN, Kowall NW, Nauta WJ (1986) Cytoarchitecture, fiber connections, and some histochemical aspects of the interpeduncular nucleus in the rat. *J Comp Neurol* 249:65–102.
10. Olucha-Bordonau FE, et al. (2003) Cytoarchitecture and efferent projections of the nucleus incertus of the rat. *J Comp Neurol* 464:62–97.
11. Shibata H, Suzuki T (1984) Efferent projections of the interpeduncular complex in the rat, with special reference to its subnuclei: A retrograde horseradish peroxidase study. *Brain Res* 296:345–349.
12. Shibata H, Suzuki T, Matsushita M (1986) Afferent projections to the interpeduncular nucleus in the rat, as studied by retrograde and anterograde transport of wheat germ agglutinin conjugated to horseradish peroxidase. *J Comp Neurol* 248:272–284.
13. Vertes RP, Fortin WJ, Crane AM (1999) Projections of the median raphe nucleus in the rat. *J Comp Neurol* 407:555–582.
14. Nuñez A, Cervera-Ferri A, Olucha-Bordonau F, Ruiz-Torner A, Teruel V (2006) Nucleus incertus contribution to hippocampal theta rhythm generation. *Eur J Neurosci* 23: 2731–2738.
15. Vertes RP, Kocsis B (1997) Brainstem-diencephalo-septohippocampal systems controlling the theta rhythm of the hippocampus. *Neuroscience* 81:893–926.
16. Klemm WR (2004) Habenular and interpeduncularis nuclei: Shared components in multiple-function networks. *Med Sci Monit* 10:RA261–RA273.
17. Gong S, et al. (2003) A gene expression atlas of the central nervous system based on bacterial artificial chromosomes. *Nature* 425:917–925.
18. Paylor R, Lindsay E (2006) Mouse models of 22q11 deletion syndrome. *Biol Psychiatry* 59:1172–1179.
19. Saint-Jore B, et al. (1998) Goosecoid-like (Gscl), a candidate gene for velocardiofacial syndrome, is not essential for normal mouse development. *Hum Mol Genet* 7:1841–1849.
20. Gottlieb S, et al. (1997) The DiGeorge syndrome minimal critical region contains a goosecoid-like (GSCL) homeobox gene that is expressed early in human development. *Am J Hum Genet* 60:1194–1201.
21. Hemmendinger LM, Moore RY (1984) Interpeduncular nucleus organization in the rat: Cytoarchitecture and histochemical analysis. *Brain Res Bull* 13:163–179.
22. Tamamaki N, et al. (2003) Green fluorescent protein expression and colocalization with calretinin, parvalbumin, and somatostatin in the GAD67-GFP knock-in mouse. *J Comp Neurol* 467:60–79.
23. Groenewegen HJ, Wouterlood FG (1988) Basal forebrain inputs to the interpeduncular nucleus in the rat studied with the *Phaseolus vulgaris*-leucoagglutinin tracing method. *Brain Res Bull* 21:643–649.
24. Herkenham M (1981) Anesthetics and the habenulo-interpeduncular system: Selective sparing of metabolic activity. *Brain Res* 210:461–466.
25. Kennedy C, et al. (1982) Local cerebral glucose utilization in non-rapid eye movement sleep. *Nature* 297:325–327.
26. McQueen JK, Martin MJ, Harmar AJ (1984) Local changes in cerebral 2-deoxyglucose uptake during alphaxalone anaesthesia with special reference to the habenulo-interpeduncular system. *Brain Res* 300:19–26.
27. Cornwall J, Cooper JD, Phillipson OT (1990) Afferent and efferent connections of the laterodorsal tegmental nucleus in the rat. *Brain Res Bull* 25:271–284.
28. Long JM, et al. (2006) Behavior of mice with mutations in the conserved region deleted in velocardiofacial/DiGeorge syndrome. *Neurogenetics* 7:247–257.
29. Fulcher BD, Phillips AJ, Robinson PA (2008) Modeling the impact of impulsive stimuli on sleep-wake dynamics. *Phys Rev E Stat Nonlin Soft Matter Phys* 78:051920.
30. Wakamiya M, Lindsay EA, Rivera-Pérez JA, Baldini A, Behringer RR (1998) Functional analysis of Gscl in the pathogenesis of the DiGeorge and velocardiofacial syndromes. *Hum Mol Genet* 7:1835–1840.
31. Gottlieb S, Hanes SD, Golden JA, Oakey RJ, Budarf ML (1998) Goosecoid-like, a gene deleted in DiGeorge and velocardiofacial syndromes, recognizes DNA with a bicoid-like specificity and is expressed in the developing mouse brain. *Hum Mol Genet* 7: 1497–1505.
32. Galili N, Nayak S, Epstein JA, Buck CA (2000) Rnf4, a RING protein expressed in the developing nervous and reproductive systems, interacts with Gscl, a gene within the DiGeorge critical region. *Dev Dyn* 218:102–111.
33. Lindsay EA, Harvey EL, Scambler PJ, Baldini A (1998) ES2, a gene deleted in DiGeorge syndrome, encodes a nuclear protein and is expressed during early mouse development, where it shares an expression domain with a Goosecoid-like gene. *Hum Mol Genet* 7:629–635.
34. Karayiorgou M, et al. (1995) Schizophrenia susceptibility associated with interstitial deletions of chromosome 22q11. *Proc Natl Acad Sci USA* 92:7612–7616.
35. International Schizophrenia Consortium (2008) Rare chromosomal deletions and duplications increase risk of schizophrenia. *Nature* 455:237–241.
36. Wang H, et al. (2006) Transmission disequilibrium test provides evidence of association between promoter polymorphisms in 22q11 gene DGCR14 and schizophrenia. *J Neural Transm* 113:1551–1561.
37. Sigurdsson T, Stark KL, Karayiorgou M, Gogos JA, Gordon JA (2010) Impaired hippocampal-prefrontal synchrony in a genetic mouse model of schizophrenia. *Nature* 464:763–767.
38. Paxinos G, Franklin KBJ (2004) *The Mouse Brain in Stereotaxic Coordinates* (Elsevier, San Diego).